The effect of experimental diabetes and glycaemic control on Guided Bone Regeneration. Histology and gene expression analyses

Retzepi M[1], Calciolari E[1], Wall I[2], Lewis MP[3] Donos N[1]

1, Centre for Oral Clinical Research, Institute of Dentistry, Queen Mary University of London (QMUL), Barts and The London School of Medicine and Dentistry, London, UK

2, Regenerative Medicine Bioprocessing Unit, UCL Advanced Centre for Biochemical Engineering, Torrington Place, London, UK

3, National Centre for Sport and Exercise Medicine, School of Sport, Exercise and Health Sciences, Loughborough University, Loughborough, UK.

Corresponding author:
Prof Nikolaos Donos, DDS, MS, FHEA, FDSRCSEngl., PhD
Centre for Clinical Oral Research
Institute of Dentistry
Queen Mary University of London (QMUL)
Barts and The London School of Medicine and Dentistry
Turner Street,
London, E1 2AD
Email: n.donos@qmul.ac.uk

Running title: Bone regeneration in controlled and uncontrolled diabetes

Keywords: bone regeneration, diabetes mellitus, histomorphometry, gene expression, animal experimentation, rats

Abstract

Objectives To investigate the effect of experimental diabetes and metabolic control on intramembranous bone healing following guided bone regeneration (GBR).

Material and methods Ninety-Three Wistar rats were allocated to three experimental groups, healthy (H), uncontrolled diabetes (D) and controlled diabetes (CD). 21 days following diabetes induction, a standardised 5-mm defect was created at the mid portion of each parietal bone. In 75 animals (25H, 25D, 25CD), one defect was treated with an intracranial and extracranial membrane according to the GBR principle, and one defect was left empty (control); five animals per group were then randomly sacrificed at 3, 7, 15, 30 and 60 days and processed for decalcified histology. In 18 animals (6H, 6D, 6CD), both defects were treated according to the GBR principle; three animals from each group were then randomly sacrificed at 7 and 15 days of healing and employed for gene expression analysis.

Results Application of the GBR therapeutic principle led to significant bone regeneration even in the D group. However, at 15 and 30 days, the osteogenesis process was impaired by uncontrolled diabetes, as shown by the significant reduction in terms of defect closure (38%-42%) and newly formed bone (54%-61%) compared to the healthy group. The comparison of the D versus H group at 15 days of healing yielded the largest number of genes with significantly differential expression, amongst which various genes associated with the ossification process (*bmp4*, *ltbp4*, *thra* and *cd276)* were identified.

Conclusions Uncontrolled diabetes seems to affect early phases of the bone regeneration following GBR. A misregulation of genes and pathways related to cell division, energy production, inflammation and osteogenesis may account for the impaired regeneration process in D rats. Further studies are warranted to optimise the GBR process in this medically compromised patient population.

Introduction

Diabetes mellitus is defined as a "group of metabolic diseases characterised by hyperglycaemia resulting from defects in insulin secretion, insulin action, or both" (American Diabetes 2014)and it is the most common chronic metabolic disease, affecting 8.5% of adults over 18 years of age (Global report on diabetes. World health organization 2016). The number of people with diabetes has risen from 108 million in 1980 to 422 million in 2014 (Global report on diabetes. World health organization 2016) and it has been estimated that between 2010 and 2030, there will be a 69% increase in the number of adults with diabetes in developing countries and a 20% increase in developed countries (Shaw, et al. 2010). The vast majority of diabetic cases falls in one of the following categories: a) Type 1 Diabetes Mellitus (T1DM), a condition characterised by absolute deficiency of insulin secretion, resulting from autoimmune destruction of the insulin producing beta cells of the pancreas; b) Type 2 Diabetes Mellitus (T2DM), a condition characterised by impaired insulin function, i.e. resistance to insulin action, combined with inadequate compensatory insulin secretion response (American Diabetes 2014).

T1DM is the result of a complex interaction between genes and environmental factors. The genetic component in T1DM aetiology is predominantly associated with high risk and/or protective HLA haplotypes, residing on the DR and DQ genotypes (Pociot & Lernmark 2016). Diabetes mellitus has been associated with the occurrence of a series of complications involving the skeletal system, collectively referred to as "diabetic bone disease" or "diabetic osteopathy" (Bouillon 1991). The diabetic skeletal phenotype presents the following features: i) diminished linear bone growth during the pubertal growth spurt in adolescents with diabetes (Bizzarri, et al. 2014, Salerno, et al. 1997); ii) reduction of bone mineral density and increased risk for occurrence of osteopenia and osteoporosis (Vestergaard 2007); iii) increased fracture risk (Janghorbani, et al. 2007); iv) poor osseous healing characteristics and impaired bone regeneration potential (Choi, et al. 2014, Cozen 1972, Liuni, et al. 2015).

A meta-analysis by Vestergaard et al (Vestergaard 2007) has shown that, although the relative risk for hip fracture is moderately increased in T2DM patients (1.38, 95% CI: 1.25–1.53), the bone mineral density in the hip and the spine is increased. On the contrary, T1DM is clearly associated with a significantly increased fracture risk (RR=6.94, 95% CI: 3.25–14.78) and a decreased bone density. Since hyperinsulinaemia is associated with increased bone mineral density, it has been hypothesised that the observed clinical dichotomy may be accounted for by the discrepancy in systemic insulin concentration between T1DM and T2DM populations, i.e. insulinopenia vs hyperinsulinaemia respectively (Thrailkill, et al. 2005). Hence, the T1DM skeletal phenotype may

represent a more straightforward system, in order to understand the effect of suppressed insulin signalling and hyperglycaemia on the regulation of bone mass and on the osseous healing process (McCabe 2007).

Suppressed differentiation, proliferation and bone forming capacity of osteoblastic cells during the critical early healing period have been implicated as plausible pathogenetic mechanisms underlying poor bone formation in T1DM (Jiao, et al. 2015, Kalaitzoglou, et al. 2016). The hyperglycaemic wound healing milieu and the accumulation of advanced glycation end-products (AGEs) have been directly implicated in the impaired ossification potential of diabetic bone (Kume, et al. 2005, McCarthy, et al. 2001, Santana, et al. 2003). Although it has been documented that abnormal bone repair in experimental diabetes is insulin dependent, because the deficient osseous healing process is reversed by insulin treatment (Goodman & Hori 1984, Hou, et al. 1993, Suzuki, et al. 2003), it is at present unclear whether this effect is primarily due to the insulin deficiency or to the hyperglycaemia characterising the diabetic status (Thrailkill, et al. 2005).

Guided Bone Regeneration (GBR) was introduced as a therapeutic modality aiming to achieve bone regeneration, via the use of barrier membranes in 1988 (for review see (Retzepi & Donos 2010)). The GBR concept is based on the Guided Tissue Regeneration principle, according to which the regeneration of a certain type of tissue is achieved when cells with the capacity to regenerate the particular type of lost tissue are allowed to selectively repopulate the defect during healing (Gottlow, et al. 1984, Nyman, et al. 1982). The GBR therapeutic protocol involves the surgical placement of a rigid, cell occlusive membrane facing the bone surface, in order to physically seal off the skeletal site in need for regeneration (Dahlin, et al. 1990, Dahlin, et al. 1988, Retzepi & Donos 2010). The membrane creates and maintains a secluded space, thus providing an environment that is permissive for the proliferation, differentiation and expression of osteoprogenitor cells. GBR, in association or not with different bone grafts, has been successfully applied for the treatment of critical size defects (CSDs) (Al-Kattan, et al. 2016, Calciolari, et al. 2016, Donos, et al. 2011a, Donos, et al. 2004), for the regeneration of peri-implant defects (Donos, et al. 2008), for socket preservation (Cardaropoli, et al. 2012, Mardas, et al. 2010) and *de novo* bone formation (neo-osteogenesis) (Hammerle, et al. 1996, Lundgren, et al. 1995, Mardas, et al. 2003), in healthy and medically compromised conditions (Donos, et al. 2015). The calvarial CSD has been widely used in bone regeneration research since it is easy to reproduce and standardize, and the presence of the dura mater and overlaying skin provide enhanced support and stabilization to biomaterials (Gomes & Fernandes 2011, Vajgel, et al. 2014). It is considered a very challenging model since in calvarial CSD the regeneration is supported only by the

proliferation and differentiation of osteopogenitor cells coming from the periphery of the defect (Mardas, et al. 2008).

The GBR model has been previously applied to study the effect of uncontrolled and systemically insulin-controlled streptozocin-induced diabetes on bone healing in rat calvarial CSDs (Shyng, et al. 2001) and on de novo bone formation in the mandible (Retzepi, et al. 2010) and calvaria of rats (Fuegl, et al. 2011, Lee, et al. 2013).

In the attempt to gain a better understanding of the pathogenic mechanisms of deficient osseous healing in T1DM, the aims of this project were to explore the effect of experimental diabetes and metabolic control on the histological features characterising the different stages of intramembranous bone healing following GBR and to correlate them to genes differentially expressed at early stages of bone healing.

Materials and Methods

Ninety-three male Wistar rats, weighing 250±20 g and approximately 8-10 weeks in age were used in this experimental study. *In vivo* procedures were conducted in accordance with the Animals Scientific Procedures Act 1986, UK and under licensure from the Home Office. ARRIVE guidelines for reporting in vivo animal experiments were followed. The rats were observed in the animal facility for at least one week preoperatively and were kept at a constant temperature of 22°C. They were maintained with a light cycle of 12 hours (6 am to 6 pm), they had ad libitum access to drinking water and to a standard laboratory diet and their body weight was weekly monitored.

Experimental diabetes induction, glycaemic control and characterisation

The animals were allocated into three experimental groups, as follows (Figure 1):

Group H: group with healthy (non-diabetic) controls;

Group D: group with uncontrolled diabetes;

Group CD: group with controlled diabetes.

At baseline, diabetes was induced in the animals of the D and CD groups, via a single intraperitoneal injection of streptozotocin (STZ) (Sigma-Aldrich, UK) dissolved in citrate buffer (0.01 M; pH 4.3) at a dose of 65 mg/kg of body weight (Bolzan & Bianchi 2002). The blood glucose levels were monitored enzymatically in tail-nicked samples via the glucose-oxidase method (Accu-Check Advantage; Roche Diagnostics, Indianapolis, US) at the following time points: prior to diabetes induction, seven days after the injection of streptozotocin (in order to

confirm diabetes onset), prior to surgical procedure (21 days after baseline) and at sacrifice. Rats with serum glucose concentrations greater than 270mg/dl (15mmol/l) were considered as diabetic. Following diabetes confirmation, the animals in the CD group were treated with subcutaneous applications of a sustained-release insulin implant using a trocar/stylet (Linplant^{TM} ©Linshin Canada INC., Scarborough, Ontario, Canda), which was aseptically placed in the dorsal neck. The sustained release insulin implant contains bovine insulin in an erodible palmitic acid matrix (14% bovine insulin, 86% palmitic acid; weight 26±2 mg/implant) and provides constant insulin release at a rate of 2 IU/day for approximately 30 days (Follak, et al. 2004). The subcutaneous placement of the systemic insulin delivery device was repeated at 30 and 60 days following the initial delivery.

Experimental Guided Bone Regeneration (GBR) model

21 days following baseline, GBR was performed. General anesthesia of the animals was accomplished by means of halothane inhalation (3% during induction; 1.5% during maintenance). Following a midline sagittal incision through the skin and the periosteum from the occipital to the frontal region of the calvarium, the cranial vertex was exposed. One standardised, bicortical, defect was created at the mid portion of each parietal bone, by means of a trephine bur (No KB-227A.204.050, General Medical, UK). The external diameter of the drilled defect was 5.0 mm, which is considered as a Critical Size Defect (CSD) in rats (Vajgel, et al. 2014). The mid-sagittal suture was not included in the bone defect, in order to preclude its contribution to the bone healing process and to limit the risk of damaging the superior sagittal sinus (Bosch, et al. 1995, Donos, et al. 2004). In 75 randomly selected animals (25 per group) the defects were treated as follows:

- test site, one defect was covered at both the extracranial and intracranial aspect with an ePTFE non-resorbale membrane (Gore-Tex regenerative membrane, Gore Medical, Arizona, US);
- control site, the contralateral defect was left untreated.

In the remaining 18 animals (6 per group) both calvarial defects were treated with intracranial and extracranial ePTFE non-resorbale barriers according to the GBR principle.

The wound was closed in layers using a resorbable suture (Vicryl® 5.0, Ethicon, Germany). Buprenorphine hydrochloride (Vetergesic, 0.3 mg/mL, Reckitt Benckiser Healthcare, UK) was administered subcutaneously at a dose of 0.04 mg/kg, and enrofloxacin (Baytril®, Bayer, Leverkusen, Germany) was administered subcutaneously at a dose of 2.5 mg/kg and continued per os at a dose of 2.5 mg/kg per day for 7 days.

Out of the 75 animals treated with a test and control defect, five animals from each experimental group (H, D and CD) were randomly sacrificed at 3, 7, 15, 30 and 60 days of healing via CO_2 asphyxiation and processed for histology and histomorphometry evaluations. Out of the 18 rats where GBR was applied in both defects, three animals from each experimental group (H, D and CD) were randomly sacrificed at 7 and 15 days of healing via CO_2 asphyxiation and employed for gene expression analysis.

Histological analysis

After euthanasia, block biopsies of 75 animals (25 per group) were prepared and the specimens were fixed in 10% formol saline, followed by decalcification in 5.5% EDTA for at least 2 weeks. Fixed and decalcified samples were dehydrated in a graded series of increasing ethanol concentrations up to 100%, transferred to xylene and embedded into paraffin. Serial sections of 5 μm were obtained perpendicularly to the cranial vertex and in anterior-posterior direction and mounted on poly-L-lysine coated slides. The sections were stained with haematoxylin and eosin. Histological examination of the specimens was performed using a Leitz DM-RBEs microscope (Leica, Heidelberg, Germany) equipped with the Image-Pro Plus v.4.5 Imaging System (Media Cybernetics, Wokingham, UK). Digital photomicrographs were obtained using a CoolsnapPRO-cf digital camera (Media Cybernetics, Marlow, Bucks, UK) connected to the microscope.

Qualitative assessment of the healing outcome was performed and classified as follows (Bosch, et al. 1995, Donos, et al. 2004):

- *no closure;* specimens in which the bone defect remained open, with the exception of minor new bone apposition at the margins of the defect;
- *partial closure;* specimens in which new bone formation had taken place from the margins of the bone defect, without establishing a complete bone continuity;
- *complete closure;* specimens in which complete osseous continuity was present between the margins of the defect.

Three central sections of the mid-portion of each defect were used for planimetric analysis. The following linear measurements were performed using the Image Pro Plus Imaging System:

- *residual defect size*; the distance between the margins of the newly formed bone in the anterior-posterior dimension excluding any isolated bone spicules present along the central axis;
- *initial defect size*; the distance delineated by the defect borders in the anterior-posterior dimension.

The *percentage of defect bridging* was also calculated as the ratio of the difference between the initial and residual defect size to the initial defect size (Bosch, et al. 1995). The mean value of the measurements performed in the three central sections was used for statistical analysis.

All linear measurements were performed by one previously calibrated examiner (MR) at a magnification x20. The reproducibility of the measurements was tested by randomly duplicating 10% of above mentioned measurements following a minimum two-week interval period. Intra-examiner reproducibility was confirmed via calculation of the intra-class correlation coefficient (ICC=0.864, 95%CI 0.779-0.876).

Morphometric evaluation was performed using the Image Pro Plus Imaging System v4.5 (Media Cybernetics, Marlow, Bucks, UK) on one section of the central portion of each specimen, at the marginal and central defect area. Three histomorphometric fields of 100 μm^2 (i.e. one central and two marginal fields) were considered and morphometric point counting was performed at original magnification of X400. The results obtained from the two marginal histomorphometric fields were averaged for each section (Bosch, et al. 1995)

In particular, the composition of the tissue within each area was analysed with respect to its content in osteoblasts, fibroblast-like mesenchymal cells, adipocytes, erythrocytes, leukocytes (including polymorphonuclear cells, lymphocytes and plasma cells), monocytes/macrophages, vascular structures, mineralised tissue components and unidentified structures (residual tissue).

Gene expression analysis using Genechip Microarrays

18 animals were used for gene expression analysis, where both calvarial defect were treated according to the GBR principle. On day 7 and 15 of healing, 3 animals per experimental group were sacrificed and the tissue within each defect was harvested and immediately submerged in 1.0ml of RNA*later* RNA Stabilization Reagent (#AM7024, Applied Biosystems/Ambion, Austin TX, USA) and stored at 4°C for a minimum of 24 h and a maximum of 72 h and eventually transferred to -20°C until RNA isolation. The details of Genechip microarray analysis are described elsewhere (Al-Kattan, et al. 2016). Briefly, after RNA isolation, quality and quantity assessment, a Two-Cycle Eukaryotic Target Labeling Assay was performed, in order to obtain sufficient amounts of labeled cRNA target for analysis with arrays, according to the manufacturer's instructions (http://www.affymetrix.com/support/technical/manual/expression_manual.affx).

The 18 samples were prepared and the cRNA was hybridised to Affymetrix GeneChip® Rat Genome 230 2.0 Arrays (Rat 230 2.0, Affymetrix, Santa Clara, CA, USA), as previously

described (Al-Kattan, et al. 2016). Following 16 hours of hybridisation, the microarrays were stained and washed on an Affymetrix GeneChip® Fluidics Station 450. The arrays were scanned on an Affymetrix GeneChip® Scanner 7G and image files called dat files were created. Based on these image files, the GeneChip® Operating Software (GCOS) computed cell intensity data (.cel files), which were analysed and saved as chp files containing data analysis information for each probe set on the arrays.

The Affymetrix MAS 5.0 software was used in order to scale the data to a target intensity of 1500 and to calculate transcript abundance. The following quality control plots were used to evaluate the Affymetrix data quality:

- boxplots in order to identify outliers by comparing medians and intensity ranges between samples;
- reproducibility between biological replicates based on density plots comparing the intensity distributions among the arrays;
- histograms of perfect match (PM) versus mismatch (MM) comparing the intensity distributions values of the PM versus the MM probes for each chip;
- RNA degradation slopes indicating potential RNA degradation and/or inefficient labeling among arrays. Genes and transcripts are represented on Affymetrix chips as a series of oligonucleotide probes. These are numbered 0-10, with probe 0 being the most 5' sequence and probe 10 the most 3' sequence. RNA degradation plots show average intensity of the probes as a function of their 5'-3' position of probes;
- MvA plots with a view to check the reproducibility of biological replicates and to indicate whether large differences in genes expression between groups should be expected in these graphs, M-values, i.e. log-2 fold change between the intensity value of each probeset in the two samples, are plotted against the A-values, i.e. the average intensity of each probeset across all the chips;
- correlation plot, a heatmap of the array-array Spearman rank correlation coefficients, has been used to detect outliers.

Statistical analysis

Statistical analysis was performed using the SPSS statistical software (SPSS 14.0, Chicago, IL, USA). The significance of differences among experimental groups in histological bone bridging and in area of regenerated bone per bone length was evaluated using the General Linear Model (GLM) univariate test, after the assumptions of homogeneity of variance and

normality of the residuals distribution were tested. The Least Significant Differences *post-hoc* test for multiple comparisons was used, in order to evaluate the differences between experimental groups within each treatment type and healing time-point. The level of statistical significance was set at 0.05. Data are reported as mean ±standard error of mean (SEM). The composition of the tissue within each area of interest in terms of osteoblasts, fibroblast-like mesenchymal cells, adipocytes, erythrocytes, leukocytes, monocytes/macrophages, vascular structures, mineralised tissue components and unidentified structures was qualitatively described and presented as 100% stacked bar charts.

Differential gene expression between experimental groups was statistically tested by using the Linear Models (LIMMA) in the Bioconductor package v1.9 and R version 2.4.0. LIMMA applies a modified t-test, which uses a Bayesian approach to make the analysis stable even for small sample numbers. Three pairwise comparisons were performed on GC Robust Multi-Array Analysis (GCRMA)-normalised data at 7 and 15 days of healing: (1) Diabetic *versus* healthy; (2) Controlled diabetic *versus* diabetic; (3) Controlled diabetic *versus* healthy. Summary statistics were compared for each gene and for each paired comparison performed.

The data p-values were corrected using the Benjamini-Hochberg test to control the false discovery rate (FDR) following multiple testing. An adjusted p-value cut-off of 0.05 was used to select differentially expressed genes, which means that all genes with an FDR-adjusted value<0.05 were considered as differentially expressed and that the expected proportion of false discoveries was controlled to be less than 5%.

Probe set annotations were derived from the NetAffx website (www.affymetrix.com). Supervised hierarchical clustering was performed using all the probesets with FDR<0.05 in any of the pair-wise statistical comparisons. The Manhattan distance metric and average linkage were used for the clustering.

Gene ontology and pathway analyses

Biological interpretation of the GeneChip® expression data was performed via pathway and Gene Ontology analysis by using the GenMAPP 2.1 software (Gene Map Annotator and Pathway Profiler), as previously described (Al-Kattan, et al. 2016). For each paired comparison, a dataset of significantly altered genes (p<0.05) presenting at least twofold change was entered into GenMAPP. The MAPPFinder and the annotations from the Gene Ontology (GO) Consortium, were used to identify underlying processes or mechanisms and global biological trends in gene expression data. More specifically, MAPPFinder calculated the relative amount of differentially expressed genes present within each MAPP/GO term and a statistical z-score of the association of gene expression changes with a particular MAPP/GO

term (Doniger, et al. 2003). A positive z- score indicates that there are more genes linked to a MAPP/ GO term than would be expected by random chance. In our analysis MAPPs with z-score>1.96 (which corresponds to a *p*-value<0.05) were considered as significantly overrepresented in the differential gene list. In order for a MAPP to be considered for further analysis, it had to include a minimum of five differentially expressed genes.

Results

Healing progressed uneventfully in all animals.

Diabetes induction and characterisation

Blood glucose measurements indicated that diabetes developed by day 7 in groups D and CD, reaching a mean value of 24.4±1.4 mmol/l and 22.3±0.9 mmol/l, respectively. The threshold level of 15mmol/l was reached in all the animals that received streptozotocin, whereas diabetes did not develop in the control animals, as expected. Hyperglycaemia was consistent and not transient, as confirmed by the blood glucose measurements during the follow-up period. Delivery of insulin pellets in the CD group led to reduction of the blood glucose values from 22.3±0.9 mmol/l at day 7, to 9.8±0.6 and 8.0±0.9 at day 21 and at sacrifice, respectively.

Histological analysis

3 days of healing

In the control sites, at 3 days of healing a blood clot occupied the original defect area, while organization of a fibrin network throughout the entire defect length was observed in all experimental groups. Numerous erythrocytes were entrapped in the fibrin mesh, while necrotic bone remnants were visible proximally to the original defect borders in some specimens. In addition, few polymorphonuclear cells (PMN) and fibroblastic cells had invaded the fibrin clot (Figure 2, a-b).

7 days of healing

At 7 days of healing, the coagulum remnants had been largely replaced by granulation tissue in both the control and test sites in all experimental groups. In the control sites of all experimental groups, neutrophils and macrophages were sparsely distributed throughout the entire defect length, engulfing damaged tissue. The average defect closure was 19.58±9.10%, 16.02±3.81% and 24.56±3.17% while the regenerated area was 0.89±0.42 mm^2, 1.27±0.57 mm^2 and 2.73±0.34 mm^2 per mm of defect length in the healthy, uncontrolled diabetic and controlled diabetic animals, respectively (Table 1).

In the GBR-treated samples, at 7 days of healing the granulation tissue formation differed in comparison to the control sites, in that it characteristically outgrew solely from the marginal bone diploe. The newly formed granulation tissue proximally to the parent bone border presented inflammatory cells and numerous fibroblast-like mesenchymal cells in a provisional, richly vascularised collagenous matrix. However, the central part of the secluded defect space presented only few fibrinous remnants, erythrocytes and scattered inflammatory cells (Figure 2, c-d). Within the GBR-treated animals, the D group showed a reduced number of PMNs (0.8%), less vascular structures (1.8%) and more abundant haematoma remnants (11.2%) proximally to the defect borders in comparison to group CD. Moreover, the central portion of the GBR treated sites in the D group presented a less organised fibrin network, with abundant erythrocytes and limited PMN (1%) (Figure 2, c-d). Morphometric analysis indicated that the provisional granulation tissue matrix in the test specimens of the CD group had a higher proportion of spindle-shape fibroblast-like cells (25.8%) and vascular structures (6%) and similar counts of inflammatory cells (1.2%) compared to the D group (Figure 2, c-d). At 7 days of healing, the average defect closure amounted to 8.78±2.31%, 5.18±1.68% and 4.35±2.50% in the healthy, uncontrolled diabetic and diabetic test animals, respectively, whereas the area of new bone was 1.04±0.56 mm^2, 0.41±0.17 mm^2 0.47±0.27 mm^2 per mm of defect length, respectively (Table 1). A significant difference in terms of defect closure ($p<0.05$) was found between the D and CD of the test and control groups.

15 days of healing

The control sites in the H and CD groups presented significant woven bone formation extending from the defect margins (28.3% and 43.1%, respectively), while the centre of the defect was filled by dense connective tissue featuring collagens fibers oriented in parallel to the long axis of the defect. The D control specimens presented limited woven bone formation, with reduced osteoblastic cells (4.9%) and vascular structures (10%) in comparison to the healthy control specimens (Figure 2, e-f). The average defect closure was 50.94±9.23%, 13.40±3.14% and 22.67±4.18% in the H, D and CD control groups, respectively, whereas the area of new bone was 8.67±1.47 mm^2, 1.63±0.41 mm^2 and 3.72±0.90 mm^2 per mm of defect length, respectively. The healthy controls presented a significantly increased defect closure and area of new bone in comparison to the controlled and uncontrolled diabetes groups ($p<0.05$) (Table 1).

At 15 days, the GBR-treated healthy (H) and controlled diabetic (CD) animals presented intense appositional bone growth originating from the defect borders and spreading towards the centre of the defect (Figure 3, a). Only limited inflammatory cells were detected, while osteoblasts, fibroblast-like cells and vascular structures were significantly observed. In five out of four GBR-

treated uncontrolled diabetic (D) rats significant new bone formation was noticed. However, the woven bone scaffold appeared as less mature in the D compared to the H group, with fewer spindle-shape fibroblast-like cells (10%) and a higher number of leucocytes (0.6%) adjacent to the defect border (Figure 2, e-f). Remarkably, in the central part of the defect, mineralised tissue was substantially decreased in the D compared to the H rats (Figure 2, e-f and Figure 3, b).

The average defect closure amounted to 44.49±6.39%, 25.48±6.00% and 35.08±2.48% in the H, D and CD test groups, respectively, whereas the area of new bone was 9.41±2.07 mm^2, 4.30±1.19 mm^2 and 7.03±1.29 mm^2 per mm of defect length, respectively (Table 1). A statistically significant reduction in both defect closure and area of new bone was found only in the D compared to the H group ($p<0.05$).

30 days of healing

Both the defect closure and the area of newly formed bone were significantly higher in the GBR-treated compared to the control animals (Table 1).

Limited new bone formation was observed in all control groups. While mineralized tissue was observed at the periphery of the defects, the central part was mainly occupied by well-organised connective tissue rich in fibroblasts. The percentage of defect closure was 26.03±5.71% in the H, 23.89±8.24% in the D and 20.68±10.88% in the CD group, while the area of regenerated bone amounted to 4.29%±0.85 mm^2, 2.73±0.60 mm^2 and 3.32±1.77 mm^2 per defect length, respectively.

All the GBR-treated sites of H and CD groups presented significant new bone formation, with clear remodeling of the woven bone into parallel fibered lamellar bone (Figure 4, a). Complete osseous union had occurred in 2 H and 1 CD specimen.

At 30 days, the GBR-treated sites in the D group presented not statistically significant reduced amounts of newly formed bone compared to the H group, with lower remodeling of the primary spongiosa into lamellar bone (Figure 4, b). Morphometric evaluation indicated that in D specimens the newly formed mineralised tissue occupied 58.2% of the defect borders and 1.7% of the central part, versus 74.8% and 26% in the H group, respectively (Figure 2, g-h). While no inflammatory cells were detected in the H specimens, in the D specimens they occupied 1.3% of the defect borders and 1% of the centre of the defect (Figure 2, g-h). The average defect closure amounted to 83.91±7.32%, 51.90±5.50% and 71.69±9.56% in the H, D and CD test groups, respectively, whereas the area of new bone was 28.22±7.85 mm^2, 11.18±1.49 mm^2 and 22.65±5.03 mm^2 per mm of defect length, respectively (Table 1). The defect closure in the D group was significantly lower than in the H group ($p<0.05$).

60 days of healing

In all control groups limited new bone formation was observed. While in the periphery of the defects mineralised tissue with a few osteocytes, vascular structures and fibroblast-rich connective tissue was observed, the central parts were mainly filled with well-organised fibrous connective tissue, with collagen fibers running in parallel to the long axis of the defect. The average defect closure amounted to 30.21±9.64%, 15.43±4.43% and 11.27±2.94% in the H, D and CD control groups, respectively, whereas the area of new bone was 5.59±1.99 mm^2, 1.45±0.44 mm^2 and 2.68±0.87 mm^2 per mm of defect length, respectively.

Likewise observed at 30 days, also at 60 days the percentage of defect closure and the area of newly formed bone were significantly higher in the GBR-treated compared to the control animals (Table 1). In the H group, marked new bone formation occupied the area between the two membranes, with obvious signs of remodeling. Two H specimens presented a complete bridge of regenerated bone (Figure 5, a). Mineralised tissue occupied 81% of the area adjacent to the defect borders and 58.8% of the central area, thus indicating a significant increase in comparison to day 30. The histology features of the CD group were similar to the H group and complete defect closure was observed in three specimens (Figure 5, b). The mineralized tissue significantly increased both in the periphery and central part of the defects (79.4% and 48.6%, respectively) (Figure 2, i-j).

Four out of five GBR treated uncontrolled diabetic (D) rats presented substantial new bone formation and complete osseous union had occurred in one specimen. Proximally to the defect border, the mineralized tissue was comparable to the healthy specimens (71.1%), although the newly mineralized tissue appeared less mature compared to the H group, it had fewer osteocytes (1.6% vs. 3%) and more abundant vascular structures (6.4% vs. 5.2%) and inflammatory cells (0.3% vs. 0%) (Figure 2, i-j and Figure 5, c). In the centre of the defect, increased new bone formation had occurred compared to 30 days, as indicate by the morphometric evaluation of mineralized tissue (26.4% vs. 1.7%) (Figure 2, i-j).

The average defect closure amounted to 82.17±5.24%, 72.00±11.66% and 77.64±14.23% in the H, D and CD test groups, respectively, whereas the area of new bone was 33.63±10.87 mm^2, 20.53±4.53 mm^2 and 50.54±15.94 mm^2 per mm of defect length, respectively (Table 1). The differences between the three groups for both parameters were not statistically significant.

RNA quality assessment

All 18 samples featured good RNA quality, with well-resolved ribosomal 18S and 28S RNA peaks and 28S/18S band ratio ≥1.8, although slight degradation was observed in some samples. All RNA samples were therefore considered reliable and utilised for transcriptomic analysis.

Quality control

Following GCRMA normalization, all box plots examining the distribution of cell intensities overlapped fairly well, thus showing that there was no large variation in the intensity values among the GeneChips and no outlier arrays were identified.

M versus A (MvA) plots showed that, although the spread of M values was large, the loess curve did not deviate significantly from the M = 0 axis, which indicated good replicate reproducibility. The intensity distributions of the PM and MM values for each GeneChip were assessed with PMvsMM histograms. All samples had typical PM and MM distributions with the cRNA binding to the MM probes less strongly then to the PM probes in all chips, thus confirming a high signal-to-noise ratio. Finally, the RNA degradation plots were used as a diagnostic tool in order to evaluate RNA quality among samples. Although the RNA degradation slopes and profiles presented limited viability among the chips, the RNA quality was similar among samples, and as such, all the samples were retained in the dataset utilised for analysis.

Differential gene expression

The number of genes with significantly differential adjusted p-value (FDR<0.05) for each pairwise comparison, are shown in Table 2. The up- and down-regulated genes for each paired comparison at 7 and 15 days of healing are presented in Table 3. The comparison of the diabetic versus the healthy group at 15 days of healing yielded the largest number of genes with significantly differential expression and was characterised by downregulation of various genes associated with the ossification process, such as *bmp4*, *ltbp4*, *thra* and *cd276*.

Hierarchical clustering

Supervised hierarchical clustering was performed on a dataset consisting of 2451 probe sets presenting an FDR value less than 0.05 (data not shown). The analysis showed a clear separation between the 7- and 15- days specimens, indicating a characteristic genetic profile related to each stage of intramembranous healing. Overall the samples of different experimental groups were separated between 7 and 15 days in terms of gene expression. Furthermore, the clustering suggested a clear separation between the D and CD specimens versus the H specimens at 15 days of healing. Similarly, at 7 days, the D and CD specimens clustered separately versus the H specimens, even though the separation was less clear.

Gene ontology

Uncontrolled diabetes versus Healthy

At day 7, 534 probes were upregulated and 230 probes were downregulated in the D versus the H group at 7 days of healing, which corresponded to 272 upregulated genes and 127 downregulated genes in the uncontrolled diabetic status, which were linked to GO terms.

At day 15, 602 probes were upregulated and 1423 probes were downregulated in the D group, which corresponded to 190 upregulated genes and 966 downregulated genes in the diabetic status, which were linked to GO terms.

A list of selected GO terms is presented in Table 4. For instance, *immune response*, *inflammatory response*, *cytokine production*, *chemokine activity* and metabolic processes (e.g. cell proliferation, regulation of cell cycle) were downregulated in the D status at day 7. Conversely, biological processes related to *negative regulation of signal transduction,* including *negative regulation of the Wnt receptor family,* were overexpressed in the D versus the H group.

At 15 days, the *regulation of developmental process*, *regulation of cell morphogenesis, regulation of angiogenesis, humoral immune response and complement activation,* as well as *cell division, cellular component organization and biogenesis, actin cytoskeleton organization and biogenesis* were downregulated in the D versus the H group. *Positive signal transduction* was also downregulated in the D group, including downregulation of the *I-kappaB kinase/NF-kappaB cascade* and the *regulation of the Wnt receptor signalling pathway*. Certain biological processes such as *leucocyte activation, lymphocyte activation, T-cell activation, mononuclear cell proliferation* and *lymphocyte proliferation* presented as upregulated in the D compared to the H group at 15 days of healing (Table 4).

Controlled diabetes versus Uncontrolled diabetes

At 7 days, 79 probes were upregulated and 76 probes were downregulated in the CD compared to the D group, which corresponded to 51 upregulated genes and 34 genes in the insulin controlled group, which were linked to GO terms.

At 15 days, insulin mediated glycaemic control was associated with upregulation of 182 probes and downregulation of 187 probes, which corresponded to 84 upregulated genes and 120 downregulated genes in the CD compared to the D group, which were linked to GO terms

A list of selected GO terms is presented in Table 4. For instance, at 7 days, insulin mediated glycaemic control was associated with significant upregulation of several GO terms related to biological processes, including *cellular organisation and biogenesis*, *cell surface receptor linked signal transduction, establishment of localization* and *transport, protein localization,*

protein transport and *vesicle mediated transport.* Conversely, *post-translational protein modification* and *phosphate metabolic process* were downregulated in the CD versus the D group at 7 days of healing.

At 15 days, *leucocyte activation*, *lymphocyte activation* and *regulation of apoptosis* were downregulated in the CD versus the D group. On the contrary, insulin mediated glycaemic control was related to upregulation of *multicellular organismal development*, *regulation of developmental process* and *anatomical structure development* (Table 4).

Controlled diabetes versus Healthy

At 7 days, 911 probes were upregulated and 384 probes downregulated in the CD compared to the H group, which corresponded to 536 upregulated genes and 200 downregulated genes that linked to GO terms in the controlled diabetic status. 307 probes were upregulated and 1120 probes were downregulated in the CD versus the H group at 15 days of healing, which corresponded to 95 upregulated genes and 770 downregulated genes in the diabetic status, which were linked to GO terms.

At 7 days, numerous biological processes were upregulated in the CD compared to the H group, such as *cell adhesion, cellular component organization and biogenesis*, *cell growth* and *cell maturation, cellular localization, intracellular transport, nuclear transport protein transport, anion transport*. In terms of signal transduction, the *transmembrane receptor protein serine/threonine kinase signalling pathway*, the *TGFb receptor signalling pathway* and the *Wnt receptor signalling pathway* were upregulated in the CD group. Furthermore, the GO terms of *developmental process, tissue remodelling, skeletal development, ossification* and *osteoblast differentiation* were upregulated in the CD versus the H group at 7 days of healing. Conversely, the biological processes of *immune response, cytokine activity, leucocyte activation, leucocyte migration, angiogenesis, blood vessel morphogenesis, cell activation* and *response to wounding* were underexpressed in the CD group compared to the H group.

At 15 days, numerous GO terms related to biological processes were downregulated in the controlled diabetic compared to the healthy group. These included *negative regulation of apoptosis, cellular localization, cellular component organization and biogenesis, actin filament-based process, microtubule-based process, ribonucleoprotein complex biogenesis and assembly, protein transport* and *proton transport*. *Regulation of angiogenesis, regulation of hydrolase activity* and *protein kinase cascade* were also underexpressed in the CD group.

Pathway analysis

Day 7

The pathways differentially expressed between the three groups at 7 days are presented in Table 5. Seven pathways were significantly enriched in genes differentially expressed in the D vs. H group at 7 days of healing (z score ≥1.96). The D group presented significant downregulation of the *cytokines and inflammatory response pathway*, the *inflammatory response pathway* and the *IL-1 NetPath 13*, whereas the *focal adhesion was* upregulated in uncontrolled diabetes (Table 5).

Seven pathways were significantly enriched in genes differentially expressed in the CD vs/ D group at 7 days (z score ≥1.96). Particularly, the *TGF beta receptor pathway*, the *IL-5 pathway* and the *T-cell receptor pathway* were upregulated in the insulin treated group (Table 5).

Five pathways were significantly enriched in genes differentially expressed in the CD versus the H group at 7 days of healing (z-score≥1.96). The insulin treated group presented significant upregulation of the *focal adhesion pathway* and downregulation of the *IL-1 pathway* compared to the healthy group (Table 5).

Day 15

At 15 days, six pathways were significantly enriched in genes differentially expressed in the D versus the H group (z-score≥1.96). Experimental uncontrolled diabetes was associated with significant downregulation of the *TNFa NF-kB pathway*, the *electron-transport chain pathway*, the *glycolysis and glyconeogenesis pathway*, the *proteasome degradation pathway* and the *complement activation classical pathway* (Table 5).

Four pathways were significantly enriched in genes differentially expressed in the CD versus the D group at 15 days of healing (z-score≥1.96), including the *T-cell receptor pathway*, which was significantly down-regulated in the insulin treated diabetic group (Table 5).

Finally, eleven pathways were significantly enriched in genes differentially expressed in the CD versus the H group at 15 days of healing (z-score≥1.96). The CD group was associated with significant downregulation of several pathways, including the *electron transport chain*, the *glycolysis and glyconeogenesis*, the *ribosomal proteins*, the *Krebs TCA cycle* and the *nucleotide metabolism* pathway (Table 5).

Discussion

This study showed that considerable bone regeneration following GBR can be obtained even in an experimental uncontrolled diabetic status, and it has provided new insights into genes and signalling pathways differently regulated in uncontrolled and insulin-controlled diabetes.

The classic model of streptozotocin-induced experimental diabetes was employed, which characteristically presents diminished insulin production and severe hyperglycaemia, thus

mimicking the human form of T1DM (Bolzan & Bianchi 2002). A model of T1DM condition was selected because T1DM is clearly associated with suppressed bone formation and may therefore serve as a more straightforward system to investigate the impact of the hyperglycaemic state and impaired insulin signalling on the bone formation process (McCabe 2007)

The GBR treated critical size rat calvarial defect model served as a "gold standard" basic model for evaluating GBR application. This model presents the advantages of being a standardised, reproducible defect and of providing a physically well defined *in vivo* chamber for investigating the intramembranous bone regeneration process following GBR treatment (Bosch, et al. 1995, Donos, et al. 2015, Donos, et al. 2004, Hammerle, et al. 1995, Vajgel, et al. 2014).

It is noteworthy that at 7 days the defect closure was higher in the control versus the test sites, whereas at 15 days, it was similar between the test and control sites in all experimental groups. We interpreted these findings of comparable or even inferior new bone formation in the GBR versus the control sites during the first two weeks of healing as a result of the contribution of osteogenic populations from the dura and the periosteum in the control sites, which were excluded in the membrane treated sites. It is well established that the dura mater in young animals contains mesesenchymal stem cells, whose differentiation into osteoprogenitor cells promotes osseous repair of calvarial defects (Hobar, et al. 1993, Wang & Glimcher 1999). In addition, preservation of the periosteum has been reported to enhance the regenerative capacity of bone by providing vascular resources and osteoprogenitor cells (Eyre-Brook 1984). Hence, although GBR treatment eventually ensures the selective population of the defect by cells originating from the parent calvarial bone, the intracranial and extracranial GBR barrier membranes may also exclude osteogenic tissue resources, which potentially contribute to the osteogenesis process during the initial healing stages. In line with these considerations, the initial increase in defect closure in the healthy control specimens, was found to drop at later healing periods, where the lack of a barrier membrane allowed the migration of non-bone forming soft tissues inside the defect.

Our histological and morphometric evaluations indicated that the uncontrolled diabetic status compromised the initial stages of the intramembranous bone regeneration process following GBR application in critical size rat calvarial defects. This is supported by histological observations of impaired formation of the fibrin meshwork, followed by suppressed inflammatory cell populations and diminished presence of mesenchymal cells in the osseous wound milieu at the end of the first postoperative week (Figure 2).

In the GBR treated sites, at 15 and 30 days of healing, the osteogenesis process was impaired in the presence of uncontrolled diabetes, which was demonstrated by a significant reduction of 38-42% in terms of defect closure and 54-61% in terms of newly formed bone surface compared to the systemically healthy group. However, the effect of diabetes on the bone regeneration potential at the membrane treated sites was less distinct at 60 days, as opposed to 15 and 30 postoperative days, since the defect closure values in the D group (72±11.7%) were no longer significantly different to the H group (82.2±2.9%) (Table 1). In other terms, this experiment indicated that, in the presence of uncontrolled diabetes, the sustained application of the GBR principle partially "rescued" the osteogenesis potential during the later stages of the GBR healing process. These findings are in agreement with previous histometric data on GBR in diabetic conditions (Lee, et al. 2013, Retzepi, et al. 2010) and confirmed the potential of the GBR application to promote bone regeneration in the presence of uncontrolled experimental diabetes.

It could be suggested that the sustained exclusion of non-osteogenic cell populations from the osseous wound via GBR application maintained an environment permissive for bone formation during the later healing stages of the diabetic osseous wound healing process. Nonetheless, the diabetic status was characterised by diminished influx and/or proliferation of the cells orchestrating the critical early osseous healing events, i.e. inflammatory, osteoprogenitor and endothelial progenitor cells, in areas distally from the osseous wound margins. Improved glycaemic control achieved via systemic insulin treatment was associated with enhanced granulation tissue formation adjacent to the parent bone margins, as indicated by the increased counts of MSCs and newly formed vascular structures at the end of the first week of healing following GBR application (see Figure 2). In the GBR treated sites, at 30 and 60 days of healing, systemic insulin mediated glycaemic control promoted the defect closure values by 32-37% and the newly formed bone surface by 63-89% compared to the uncontrolled diabetic condition, thus conferring comparable bone regeneration potential to the healthy animals (Table 1).

Further to the histologic observations of deficient granulation tissue formation and osteogenesis during the critical initial phases following GBR application in the diabetic status, we sought to explore on a molecular level the potentially implicated pathways and to gain insight into the mechanisms via which insulin mediated glycaemic control improves the early osseous wound healing parameters. Gene expression analysis was performed only at 7 and 15 days of healing because previous studies indicated that these early time points are critical for

skeletogenesis and guided bone regeneration, since they are located in the stage where the initial inflammation is gradually overlapped by a progressive maturation of the granulation tissue into woven bone (Donos, et al. 2011b, Ivanovski, et al. 2011).

At 7 days of healing, the uncontrolled diabetic status was characterised by under-representation of pathways associated with the inflammatory and immune responses (Table 5). More specifically, gene expression profiling indicated impaired expression of genes encoding chemoattractants, such as pro-inflammatory cytokines (Il1a, Il1b, Il6, TNF), chemokines (Ccl20, Cxcl1, Cxcl2, Cxcl10), chemokine receptors (Ccr2, Ccr5, Ccr6), and cell adhesion molecules (Vcam1 and Icam1), all of which are implicated in the migration and activation of inflammatory and mesenchymal cells (Tanaka, et al. 1995, Yellowley 2013). Moreover, a downregulation of the NF-kB signalling cascade was found in the D group at 7 and 15 days of healing. The NF-kB family of transcription factors regulates the transcription of genes encoding key effector molecules for immune and inflammatory responses, such as cytokines, adhesion molecules and chemokines (Hayden, et al. 2006, Li & Lin 2008). Hence, it may be suggested that deficient NF-kB signalling and concomitantly reduced concentrations of chemoattractants in the diabetic osseous healing chamber during early granulation tissue formation may be implicated in aberrant recruitment of inflammatory and mesenchymal cells and therefore account for their diminished presence in the central parts of the osseous wound. It may be further suggested that these observations could relate to the increased risk for infectious complications following GBR treatment in the presence of uncontrolled diabetes.

At 15 days of healing, the inflammatory response was more prominent in the D compared to the H group. More specifically, the *T-cell receptor pathway*, the *leucocyte activation*, the *lymphocyte activation*, the *T-cell activation*, *the mononuclear cell proliferation* and the *lymphocyte proliferation* were overexpressed in the uncontrolled diabetic animals versus the healthy controls. Therefore, our results indicated that a delayed and prolonged inflammatory response characterised the osseous wound healing events in the diabetic status, which is in accordance with evidence from Lee et al (Lee, et al. 2016), who have shown that experimental T1DM significantly increases the expression of pro-inflammatory cytokines during the regeneration of calvarial CSDs according to the GBR principle. Furthermore, our observations are in accordance with a recent clinical study demonstrating that pro-inflammatory cytokines and chemokines were upregulated in T2DM patients with bone fracture, as well as in osteoblasts subjected to high glucose stimulation (Sun, et al. 2016).

An anti-inflammatory effect of insulin treatment on the gene profile expressed was evidenced by downregulation of the *T-cell receptor pathway*, the *IL-6 pathway*, the *leucocyte activation* and the *lymphocyte activation* in the CD compared to the D group at 15 days of healing. These data are in line with previous evidence that insulin downregulates the production of pro-inflammatory cytokines (IL-1, IL6, TNFα) via NF-kB inhibition (Dandona, et al. 2001, Sun, et al. 2014), while other studies did not confirm this finding (Pradhan, et al. 2009).

Furthermore, our gene expression analysis results are in agreement with our histomorphometric observations that the GBR treated sites in the CD group presented fewer inflammatory cells in the newly formed woven bone proximally to original defect margins at 15 days of healing compared to the uncontrolled diabetic animals.

The diabetes effect on the gene profiles expressed by the cells populating the osseous wound chamber was most prominent at 15 days and characteristically featured downregulation of cell division and of several energy-producing metabolic pathways. These results correlate with our histological observations of reduced numbers of MSCs and osteoblastic cells in the central parts of the GBR treated defects in the diabetic group at 15 days of healing (Figure 2, e-f).

Remarkably, a series of genes implicated in the osteogenic process were identified as significantly downregulated in uncontrolled diabetes, including bone morphogenetic protein 4, latent transforming growth factor beta binding protein 4, thyroid hormone receptor alpha and CD276 antigen. Misregulation of these osteogenesis related genes may be directly implicated in the histologically observed impaired osteogenesis potential observed at 15 days of healing following GBR application. Furthermore, Wnt signalling pathway, which plays a major role in osteoblast commitment and differentiation and skeletogenesis (Glass, et al. 2005, Monroe, et al. 2012), was misregulated in the diabetic status at 7 and 15 days and, as such, it may be also implicated in the deficient expression of genes involved in the cell division pathway in the diabetic status. Notably, Anagnostou and Shepherd (Anagnostou & Shepherd 2008) have also provided evidence indicating that the Wnt/beta-catenin system is a glucose-responsive signalling system and suggested that the Wnt signalling cascade could be misregulated in the hyperglycaemic status. The Wnt-Frizzled signal transduction may therefore constitute a plausible molecular link between uncontrolled diabetes and aberrant cell proliferation during the intramembranous bone healing process following GBR application.

This study presents with some limitations. This animal model allowed to investigate only short-term effects of insulin deficiency, without taking into account potential consequences on bone healing related to the long-term consequences of uncontrolled diabetes (e.g. vasculopathy). Although genome-wide transcriptomic analyses provide important data about the molecular

mechanisms associated to a biological process, the levels of mRNA are not directly proportional to the expression level of the proteins they code for. The future step will be to combine these results with proteomic data, to have a broader and more precise picture of the mechanisms involved in bone regeneration and of the effect of diabetes at the different stages. In an attempt to extrapolate our results to a clinical setting, one should consider the higher variability of the treatment outcome in the uncontrolled diabetic status, which is probably related to aberrations during the early phases of the osseous healing process. Consequently, further studies are warranted aiming to optimise the GBR process in this medically compromised patient population. In this context, investigation of the benefits from the use of biomaterials with enhanced osteoinductive or osteoconductive properties for the reconstruction of osseous defects in diabetic patients is necessary.

Carefully designed studies addressing the impact of T2DM and the related higher bone mineral density, insulin resistance and obesity to the pathophysiology of the healing process following GBR application are also warranted.

Acknowledgments

The authors do not have any conflict of interest.

MPL's contribution to this activity was conducted under the auspices of the National Centre for Sport and Exercise Medicine (NCSEM) England, a collaboration between several universities, NHS trusts and sporting and public bodies. The views expressed are those of the authors and not necessarily those of NCSEM England or the partners involved.

Figure legend

Figure 1 The flow chart describes the study design and the number of animals used. CD, controlled diabetes; D, uncontrolled diabetes; H, healthy controls; GBR, guided bone regeneration.

Figure 2 Results of the morphometric analysis of the GBR treated sites. Assessments were performed in areas located proximally to the defect margins and in the centre of the defect on postoperative days 3 (a-b), 7 (c-d), 15 (e-f), 30 (g-h) and 60 (i-j). Data are presented as 100% stacked bar charts.

Figure 3 Photomicrographs of GBR treated specimens at 15 days of healing. a, Detail of a healthy specimen. Trabecular bone scaffold with evident formation of primary osteons and

numerous osteocytes embedded in the mineralised tissue in the area proximally to the defect border. Remodelling activity is observed proximally to the defect border. b, Detail of an uncontrolled diabetes specimen. Immature woven bone and sinusoidal capillaries (black arrows) present proximally to the defect border. The original defect borders are demarcated by the black arrowheads. PO, primary osteons; VS, vascular structures. Stained with H&E, original magnification X400.

Figure 4 a, Detail of GBR treated healthy specimen at 30 days of healing. Maturation of woven bone into lamellar bone and formation of secondary osteons (SO) are observed at the periphery of the defect. b, Detail of a GBR treated uncontrolled diabetes specimen at 30 days of healing. Connective tissue (CT) is still present among the islands of new bone in the area proximally to the defect border. The original defect borders are demarcated by arrows. Stain H&E, original magnification X400.

Figure 5 Photomicrographs of GBR treated specimens at 60 days of healing. a, healthy specimen. Complete osseous union has occurred; the newly formed bone has largely remodelled into lamellar bone especially at the peripheral areas of the defect. b, uncontrolled diabetes specimen. Substantial bone regeneration is observed leading to partial defect closure in the presence of uncontrolled diabetes. c, controlled diabetes specimen. complete defect bridging has occurred along the original defect margins. The regenerated bone has substantially remodelled into lamellar bone. The original defect borders are demarcated by arrows. Original magnification x20. Stained with H&E.

Table legend

Table 1 Planimetric measurements of % defect closure and new bone surface per mm of defect length at 3, 7, 15, 30 and 60 days of healing in all experimental groups. Data presented as mean (standard error, SE). ┼ $P<0.05$ versus the non-GBR treated (control) site; a $P<0.05$ versus the healthy group.

Table 2 Number of genes significantly up and down-regulated in pairwise comparisons at 7 and 15 days of healing (FDR<0.05).

Table 3 Genes with significantly (FDR<0.05) differential expression in pairwise comparisons at 7 and 15 days of healing. FC, fold change.

Table 4 Selected GO terms significantly overrepresented at 7 and 15 days of healing. In red are the downregulated GO terms in uncontrolled diabetes (D), while in green are the upregulated GO terms in controlled diabetes (CD).

Table 5 Significantly enriched pathways (z-score>1.96) with genes presenting significantly differential expression ($p<0.05$) and minimum two-fold change at the 7 and 15 days of healing. A criterion of minimum 3 genes with significantly differential expression was applied for pathway selection. The percentage of differentially expressed genes (% changed), the percentage of genes present in each specific pathway (% present) and the Z score are presented. CD, controlled diabetes; D, uncontrolled diabetes; H, healthy controls; GBR, guided bone regeneration. Green is upregulated in D, orange is downregulated in D, blue is upregulated in CD and pink is downregulated in CD.

References

Al-Kattan, R., Retzepi, M., Calciolari, E. & Donos, N. (2016) Microarray gene expression during early healing of gbr-treated calvarial critical size defects. *Clinical Oral Implants Research*. Sep 11. doi: 10.1111/clr.12949.

American Diabetes, A. (2014) Diagnosis and classification of diabetes mellitus. *Diabetes Care* **37** Suppl 1: S81-90.

Anagnostou, S. H. & Shepherd, P. R. (2008) Glucose induces an autocrine activation of the wnt/beta-catenin pathway in macrophage cell lines. *Biochemical Journal* **416**: 211-218.

Bizzarri, C., Benevento, D., Giannone, G., Bongiovanni, M., Anziano, M., Patera, I. P., Cappa, M. & Cianfarani, S. (2014) Sexual dimorphism in growth and insulin-like growth factor-i in children with type 1 diabetes mellitus. *Growth Hormone & IGF Research* **24**: 256-259.

Bolzan, A. D. & Bianchi, M. S. (2002) Genotoxicity of streptozotocin. *Mutation Research* **512**: 121-134.

Bosch, C., Melsen, B. & Vargervik, K. (1995) Guided bone regeneration in calvarial bone defects using polytetrafluoroethylene membranes. *The Cleft Palate Craniofacial Journal* **32**: 311-317.

Bouillon, R. (1991) Diabetic bone disease. *Calcified Tissue International* **49**: 155-160.

Calciolari, E., Mardas, N., Dereka, X., Kostomitsopoulos, N., Petrie, A. & Donos, N. (2016) The effect of experimental osteoporosis on bone regeneration: Part 1, histology findings. *Clinical Oral Implants Research*.

Cardaropoli, D., Tamagnone, L., Roffredo, A., Gaveglio, L. & Cardaropoli, G. (2012) Socket preservation using bovine bone mineral and collagen membrane: A randomized controlled clinical trial with histologic analysis. *International Journal of Periodontics & Restorative Dentistry* **32**: 421-430.

Choi, W. J., Lee, J. S., Lee, M., Park, J. H. & Lee, J. W. (2014) The impact of diabetes on the short- to mid-term outcome of total ankle replacement. *Bone Joint Journal* **96-B**: 1674-1680.

Cozen, L. (1972) Does diabetes delay fracture healing? *Clinical Orthopaedics & Related Research* **82**: 134-140.

Dahlin, C., Gottlow, J., Linde, A. & Nyman, S. (1990) Healing of maxillary and mandibular bone defects using a membrane technique. An experimental study in monkeys. *Scandinavian Journal of Plastic and Reconstructive Surgery and Hand Surgery* **24**: 13-19.

Dahlin, C., Linde, A., Gottlow, J. & Nyman, S. (1988) Healing of bone defects by guided tissue regeneration. *Plastic and Reconstructive Surgery* **81**: 672-676.

Dandona, P., Aljada, A., Mohanty, P., Ghanim, H., Hamouda, W., Assian, E. & Ahmad, S. (2001) Insulin inhibits intranuclear nuclear factor kappab and stimulates ikappab in mononuclear cells in obese subjects: Evidence for an anti-inflammatory effect? *The Journal of Clinical Endocrinology & Metabolism* **86**: 3257-3265.

Doniger, S. W., Salomonis, N., Dahlquist, K. D., Vranizan, K., Lawlor, S. C. & Conklin, B. R. (2003) Mappfinder: Using gene ontology and genmapp to create a global gene-expression profile from microarray data. *Genome Biology* **4**: R7.

Donos, N., Dereka, X. & Mardas, N. (2015) Experimental models for guided bone regeneration in healthy and medically compromised conditions. *Periodontology 2000* **68**: 99-121.

Donos, N., Graziani, F., Mardas, N. & Kostopoulos, L. (2011a) The use of human hypertrophic chondrocytes-derived extracellular matrix for the treatment of critical-size calvarial defects. *Clinical Oral Implants Research* **22**: 1346-1353.

Donos, N., Lang, N. P., Karoussis, I. K., Bosshardt, D., Tonetti, M. & Kostopoulos, L. (2004) Effect of gbr in combination with deproteinized bovine bone mineral and/or enamel matrix proteins on the healing of critical-size defects. *Clinical Oral Implants Research* **15**: 101-111.
Donos, N., Mardas, N. & Chadha, V. (2008) Clinical outcomes of implants following lateral bone augmentation: Systematic assessment of available options (barrier membranes, bone grafts, split osteotomy). *Journal of Clinical Periodontology* **35**: 173-202.
Donos, N., Retzepi, M., Wall, I., Hamlet, S. & Ivanovski, S. (2011b) In vivo gene expression profile of guided bone regeneration associated with a microrough titanium surface. *Clinical Oral Implants Research* **22**: 390-398.
Eyre-Brook, A. L. (1984) The periosteum: Its function reassessed. *Clinical Orthopaedic and Related Research*: 300-307.
Follak, N., Kloting, I., Wolf, E. & Merk, H. (2004) Improving metabolic control reverses the histomorphometric and biomechanical abnormalities of an experimentally induced bone defect in spontaneously diabetic rats. *Calcified Tissue International* **74**: 551-560.
Fuegl, A., Tangl, S., Keibl, C., Watzek, G., Redl, H. & Gruber, R. (2011) The impact of ovariectomy and hyperglycemia on graft consolidation in rat calvaria. *Clinical Oral Implants Research* **22**: 524-529.
Glass, D. A., 2nd, Bialek, P., Ahn, J. D., Starbuck, M., Patel, M. S., Clevers, H., Taketo, M. M., Long, F., McMahon, A. P., Lang, R. A. & Karsenty, G. (2005) Canonical wnt signaling in differentiated osteoblasts controls osteoclast differentiation. *Developmental Cell* **8**: 751-764.
Global report on diabetes. World health organization (2016), Geneva, Switzerland
Gomes, P. S. & Fernandes, M. H. (2011) Rodent models in bone-related research: The relevance of calvarial defects in the assessment of bone regeneration strategies. *Laboratory Animals* **45**: 14-24.
Goodman, W. G. & Hori, M. T. (1984) Diminished bone formation in experimental diabetes. Relationship to osteoid maturation and mineralization. *Diabetes* **33**: 825-831.
Gottlow, J., Nyman, S., Karring, T. & Lindhe, J. (1984) New attachment formation as the result of controlled tissue regeneration. *Journal of Clinical Periodontology* **11**: 494-503.
Hammerle, C. H., Schmid, J., Lang, N. P. & Olah, A. J. (1995) Temporal dynamics of healing in rabbit cranial defects using guided bone regeneration. *Journal of Oral & Maxillofacial Surgery* **53**: 167-174.
Hammerle, C. H., Schmid, J., Olah, A. J. & Lang, N. P. (1996) A novel model system for the study of experimental guided bone formation in humans. *Clinical Oral Implants Research* **7**: 38-47.
Hayden, M. S., West, A. P. & Ghosh, S. (2006) Nf-kappab and the immune response. *Oncogene* **25**: 6758-6780.
Hobar, P. C., Schreiber, J. S., McCarthy, J. G. & Thomas, P. A. (1993) The role of the dura in cranial bone regeneration in the immature animal. *Plastic Reconstructive Surgery* **92**: 405-410.
Hou, J. C., Zernicke, R. F. & Barnard, R. J. (1993) Effects of severe diabetes and insulin on the femoral neck of the immature rat. *Journal of Orthopaedic Research* **11**: 263-271.
Ivanovski, S., Hamlet, S., Retzepi, M., Wall, I. & Donos, N. (2011) Transcriptional profiling of "guided bone regeneration" in a critical-size calvarial defect. *Clinical Oral Implants Research* **22**: 382-389.
Janghorbani, M., Van Dam, R. M., Willett, W. C. & Hu, F. B. (2007) Systematic review of type 1 and type 2 diabetes mellitus and risk of fracture. *American Journal of Epidemiology* **166**: 495-505.

Jiao, H., Xiao, E. & Graves, D. T. (2015) Diabetes and its effect on bone and fracture healing. *Current Osteoporosis Reports* **13**: 327-335.
Kalaitzoglou, E., Popescu, I., Bunn, R. C., Fowlkes, J. L. & Thrailkill, K. M. (2016) Effects of type 1 diabetes on osteoblasts, osteocytes, and osteoclasts. *Current Osteoporosis Reports*.
Kume, S., Kato, S., Yamagishi, S., Inagaki, Y., Ueda, S., Arima, N., Okawa, T., Kojiro, M. & Nagata, K. (2005) Advanced glycation end-products attenuate human mesenchymal stem cells and prevent cognate differentiation into adipose tissue, cartilage, and bone. *Journal of Bone and Mineral Research* **20**: 1647-1658.
Lee, R. S., Hamlet, S. M. & Ivanovski, S. (2016) The influence of titanium surface characteristics on macrophage phenotype polarization during osseous healing in type i diabetic rats: A pilot study. *Clinical Oral Implants Research*.
Lee, S. B., Retzepi, M., Petrie, A., Hakimi, A. R., Schwarz, F. & Donos, N. (2013) The effect of diabetes on bone formation following application of the gbr principle with the use of titanium domes. *Clinical Oral Implants Research* **24**: 28-35.
Li, H. & Lin, X. (2008) Positive and negative signaling components involved in tnfalpha-induced nf-kappab activation. *Cytokine* **41**: 1-8.
Liuni, F. M., Rugiero, C., Feola, M., Rao, C., Pistillo, P., Terracciano, C., Giganti, M. G. & Tarantino, U. (2015) Impaired healing of fragility fractures in type 2 diabetes: Clinical and radiographic assessments and serum cytokine levels. *Aging Clinical and Experimental Research* **27** Suppl 1: S37-44.
Lundgren, D., Lundgren, A. K., Sennerby, L. & Nyman, S. (1995) Augmentation of intramembraneous bone beyond the skeletal envelope using an occlusive titanium barrier. An experimental study in the rabbit. *Clinical Oral Implants Research* **6**: 67-72.
Mardas, N., Chadha, V. & Donos, N. (2010) Alveolar ridge preservation with guided bone regeneration and a synthetic bone substitute or a bovine-derived xenograft: A randomized, controlled clinical trial. *Clinical Oral Implants Research* **21**: 688-698.
Mardas, N., Kostopoulos, L., Stavropoulos, A. & Karring, T. (2003) Evaluation of a cell-permeable barrier for guided tissue regeneration combined with demineralized bone matrix. *Clinical Oral Implants Research* **14**: 812-818.
Mardas, N., Stavropoulos, A. & Karring, T. (2008) Calvarial bone regeneration by a combination of natural anorganic bovine-derived hydroxyapatite matrix coupled with a synthetic cell-binding peptide (pepgen): An experimental study in rats. *Clinical Oral Implants Research* **19**: 1010-1015.
McCabe, L. R. (2007) Understanding the pathology and mechanisms of type i diabetic bone loss. *Journal of Cellular Biochemistry* **102**: 1343-1357.
McCarthy, A. D., Etcheverry, S. B., Bruzzone, L., Lettieri, G., Barrio, D. A. & Cortizo, A. M. (2001) Non-enzymatic glycosylation of a type i collagen matrix: Effects on osteoblastic development and oxidative stress. *BMC Cell Biology* **2**: 16.
Monroe, D. G., McGee-Lawrence, M. E., Oursler, M. J. & Westendorf, J. J. (2012) Update on wnt signaling in bone cell biology and bone disease. *Gene* **492**: 1-18.
Nyman, S., Lindhe, J., Karring, T. & Rylander, H. (1982) New attachment following surgical treatment of human periodontal disease. *Journal of Clinical Periodontology* **9**: 290-296.
Pociot, F. & Lernmark, A. (2016) Genetic risk factors for type 1 diabetes. *Lancet* **387**: 2331-2339.
Pradhan, A. D., Everett, B. M., Cook, N. R., Rifai, N. & Ridker, P. M. (2009) Effects of initiating insulin and metformin on glycemic control and inflammatory biomarkers among patients with type 2 diabetes: The lancet randomized trial. *JAMA* **302**: 1186-1194.

Retzepi, M. & Donos, N. (2010) Guided bone regeneration: Biological principle and therapeutic applications. *Clinical Oral Implants Research* **21**: 567-576.
Retzepi, M., Lewis, M. P. & Donos, N. (2010) Effect of diabetes and metabolic control on de novo bone formation following guided bone regeneration. *Clinical Oral Implants Research* **21**: 71-79.
Salerno, M., Argenziano, A., Di Maio, S., Gasparini, N., Formicola, S., De Filippo, G. & Tenore, A. (1997) Pubertal growth, sexual maturation, and final height in children with iddm. Effects of age at onset and metabolic control. *Diabetes Care* **20**: 721-724.
Santana, R. B., Xu, L., Chase, H. B., Amar, S., Graves, D. T. & Trackman, P. C. (2003) A role for advanced glycation end products in diminished bone healing in type 1 diabetes. *Diabetes* **52**: 1502-1510.
Shaw, J. E., Sicree, R. A. & Zimmet, P. Z. (2010) Global estimates of the prevalence of diabetes for 2010 and 2030. *Diabetes Research and Clinical Practice* **87**: 4-14.
Shyng, Y. C., Devlin, H. & Sloan, P. (2001) The effect of streptozotocin-induced experimental diabetes mellitus on calvarial defect healing and bone turnover in the rat. *International Journal of Oral & Maxillofacial Surgery* **30**: 70-74.
Sun, M., Yang, J., Wang, J., Hao, T., Jiang, D., Bao, G. & Liu, G. (2016) Tnf-alpha is upregulated in t2dm patients with fracture and promotes the apoptosis of osteoblast cells in vitro in the presence of high glucose. *Cytokine* **80**: 35-42.
Sun, Q., Li, J. & Gao, F. (2014) New insights into insulin: The anti-inflammatory effect and its clinical relevance. *World Journal of Diabetes* **5**: 89-96.
Suzuki, K., Miyakoshi, N., Tsuchida, T., Kasukawa, Y., Sato, K. & Itoi, E. (2003) Effects of combined treatment of insulin and human parathyroid hormone(1-34) on cancellous bone mass and structure in streptozotocin-induced diabetic rats. *Bone* **33**: 108-114.
Tanaka, Y., Morimoto, I., Nakano, Y., Okada, Y., Hirota, S., Nomura, S., Nakamura, T. & Eto, S. (1995) Osteoblasts are regulated by the cellular adhesion through icam-1 and vcam-1. *Journal of Bone and Mineral Research* **10**: 1462-1469.
Thrailkill, K. M., Lumpkin, C. K., Jr., Bunn, R. C., Kemp, S. F. & Fowlkes, J. L. (2005) Is insulin an anabolic agent in bone? Dissecting the diabetic bone for clues. *American Journal of Physiology Endocrinology and Metabolism* **289**: E735-745.
Vajgel, A., Mardas, N., Farias, B. C., Petrie, A., Cimoes, R. & Donos, N. (2014) A systematic review on the critical size defect model. *Clinical Oral Implants Research* **25**: 879-893.
Vestergaard, P. (2007) Discrepancies in bone mineral density and fracture risk in patients with type 1 and type 2 diabetes--a meta-analysis. *Osteoporosis International* **18**: 427-444.
Wang, J. & Glimcher, M. J. (1999) Characterization of matrix-induced osteogenesis in rat calvarial bone defects: Ii. Origins of bone-forming cells. *Calcified Tissue International* **65**: 486-493.
Yellowley, C. (2013) Cxcl12/cxcr4 signaling and other recruitment and homing pathways in fracture repair. *Bonekey Reports* **2**: 300.

EXPERIMENTAL GROUP	DEFECT CLOSURE (%)	NEW BONE SURFACE PER mm (mm)
3 days		
Control		
Healthy	-	-
Diabetes	-	-
Controlled Diabetes	-	-
Test		
Healthy	-	-
Diabetes	-	-
Controlled Diabetes	-	-
7 days		
Control		
Healthy	19.58 (9.10)	0.89(0.42)
Diabetes	16.02 (3.81)	1.27 (0.57)
Controlled Diabetes	24.56 (3.17)	2.73 (0.34) [a]
Test		
Healthy	8.78 (2.31)	1.04 (0.56)
Diabetes	5.18 (1.68) [†]	0.41 (0.17)
Controlled Diabetes	4.35 (2.50) [†]	0.47 (0.27) [†]
15 days		
Control		
Healthy	50.94 (9.23)	8.67 (1.47)
Diabetes	13.40 (3.14) [a]	1.63 (0.41) [a]
Controlled Diabetes	22.67 (4.18) [a]	3.72 (0.90) [a]
Test		
Healthy	44.49 (6.39)	9.41 (2.07)
Diabetes	25.48 (6.00) [a]	4.30 (1.19) [a]
Controlled Diabetes	35.08 (2.48) [†]	7.03 (1.29)
30 days		
Control		
Healthy	26.03 (5.71)	4.29 (0.85)
Diabetes	23.89 (8.24)	2.73 (0.60)
Controlled Diabetes	20.68 (10.88)	3.32 (1.77)
Test		
Healthy	83.91 (7.32) [†]	28.22 (7.85) [†]
Diabetes	51.90 (5.50) [†a]	11.18 (1.49) [†]
Controlled Diabetes	71.69 (9.56) [†]	22.65 (5.03) [†]
60 days		
Control		
Healthy	30.21 (9.64)	5.59 (1.99)
Diabetes	15.43 (4.43)	1.45 (0.44) [a]
Controlled Diabetes	11.27 (2.94)	2.68 (0.87)
Test		
Healthy	82.17 (5.24) [†]	33.63 (10.87) [†]
Diabetes	72.00 (11.66) [†]	20.53 (4.53) [†]
Controlled	77.64 (14.23) [†]	50.54 (15.94) [†]

Table 1

	7 Days			15 Days		
	D vs H	CD vs D	CD vs H	D vs H	CD vs D	CD vs H
Downregulated	2	0	5	12	7	3
No change	31097	31099	31091	31077	31090	31093
Upregulated	0	0	3	10	2	3

Table 2

	ID	Symbol	Description	Fold Change
	7 days			
D vs H	1378172_at	Phactr2	phosphatase and actin regulator 2	-1.92
	1393933_at	Sorl1_predicted	sortilin-related receptor, L(DLR class) A repeats-containing (predicted)	-5.74
CD vs H	1378172_at	Phactr2	phosphatase and actin regulator 2	-1.94
	1390757_at	RGD1566355_predicted	similar to cell division cycle 2-like 1 (predicted)	-5.9
	1393933_at	Sorl1_predicted	sortilin-related receptor, L(DLR class) A repeats-containing (predicted)	-6.15
	1385605_at	LOC688730	similar to G protein-coupled receptor 84	-21.1
	1386346_at	Tmem19	transmembrane protein 19	2.36
	1379072_at	LOC678739	similar to phosphorylase kinase alpha 2	2.06
	1375669_at	Fkbp2_predicted	FK506 binding protein 2 (predicted)	1.79
	1375228_at	Brd2	bromodomain containing 2	-1.48
	15 days			
D vs H	1379530_at	LOC316052	eomesodermin	4.23
	1397563_at			1.8
	1397854_at			1.93
	1397384_at	LOC499124	mouse zinc finger protein 14-like	1.69
	1390757_at	RGD1566355_ predicted	similar to cell division cycle 2-like 1 (predicted)	4.53
	1371056_at	Neo1	Neogenin	-2.31
	1387232_at	Bmp4	Bone morphogenetic protein 4	-5.66
	1387874_at	Dbp	D site albumin promoter binding protein	-13.4
	1381477_at			3.39
	1368346_at	B3galt4	UDP-Gal:betaGlcNAc beta 1,3-galactosyltransferase, polypeptide 4	-4.53
	1379222_at	Ltbp4	latent transforming growth factor beta binding protein 4	-2.17
	1372617_at	RGD1566094_predicted	similar to BTB (PO)Z domain containing 2 (predicted)	-2.16
	1396145_at	Sept6_predicted	septin 6 (predicted)	-3.18
	1380313_at	Klre1	killer cell lectin-like receptor, family E, member 1	2.08
	1373539_at			-1.88
	1371017_at	Gpam	glycerol-3-phosphate acyltransferase, mitochondrial	-2.28
	1367726_at	Thra	thyroid hormone receptor alpha	-4.03
	1388333_at	Rbx1	Ring-box 1	-1.67
	1394627_at	Snx19_predicted	sorting nexin 19 (predicted)	-2.89
	1386495_at	RGD1311624	similar to KIAA0339 protein	1.34
	1387194_at	Centa1	centaurin, alpha 1	1.86

	1395737_at	Cd276	CD276 antigen	-4.38
CD vs D	1394571_at			1.99
	1379530_at	LOC316052	eomesodermin	4.08
	1394578_at	Gria2	glutamate receptor, ionotropic, AMPA2	3.07
	1397563_at			-1.76
	1397384_at	LOC499124	mouse zinc finger protein 14-like	-1.8
	1397854_at			-1.86
	1371017_at	Gpam	glycerol-3-phosphate acyltransferase, mitochondrial	-2.58
	1395048_at			-1.95
	1384764_at	RGD1563574_predicted	similar to Hypothetical protein MGC30332 (predicted)	-2.68
CD vs H	1394571_at			2.13
	1394578_at	Gria2	glutamate receptor, ionotropic, AMPA2	3.76
	1390757_at	RGD1566355_predicted	similar to cell division cycle 2-like 1 (predicted)	6.77
	1387232_at	Bmp4	bone morphogenetic protein 4	-7.62
	1371056_at	Neo1	Neogenin	-2.41
	1388333_at	Rbx1	Ring-box 1	-1.81

Table 3

UNCONTROLLED DIABETES vs HEALTHY		***UNCONTROLLED DIAB***
7 DAYS	15 DAYS	7 DAYS
Cellular localization	Cellular localization	Establishment of localization and trans
Positive regulation of signal transduction • I-kappaB kinase/NF-kappaB cascade	Transport	Cellular component organisation and biogenesis
Cell proliferation	Cellular component organization & biogenesis	Cell surface receptor linked signal transduction
Cell migration	Cell division	Cellular metabolic process
Lymphocyte activation	Positive regulation of signal transduction • I-kappaB kinase/NF-kappaB cascade • Wnt receptor signalling pathway	Immune system process
Immune response	Cellular respiration	Nucleotide binding
Inflammatory response	Carbohydrate metabolic process	Cytoplasmic part
Positive regulation of metabolic process • Positive regulation of nucleotide metabolic process • Positive regulation of protein metabolic process)	Nucleotide metabolic process	Protein complex
Binding • Chemokine receptor binding • GTP binding	Humoral immune response	Cell projection
Cell growth	Regulation of developmental process	Cytoskeleton
Negative regulation of signal transduction	Regulation of cell morphogenesis	Extracellular part
Skeletal development	Catalytic activity	
	Intracellular organelles • Mitochondrion • Golgi apparatus • Endoplasmic reticulum • Cytoskeleton	
	Protein complex	
	Lymphocyte activation	
	Lymphocyte proliferation	
	RNA metabolic process	
	Ribonucleoprotein complex	

Table 4

	7 DAYS			
	MAPP Name	**% changed**	**% present**	**Z Score**
D vs. H	Rn Cytokines_and_Inflammatory_Response_Biocarta	21.7	92	3.737
	Rn Adipogenesis	10.7	91.7	3.025
	Rn Inflammatory_Response_Pathway	16.2	92.5	3.191
	Rn Matrix_Metalloproteinases	17.4	82.1	2.77
	Rn Eicosanoid_Synthesis	17.6	94.4	2.427
	Rn IL-1_NetPath_13	13.9	97.3	2.498
	Rn Focal_adhesion_KEGG	9.3	87.5	2.656
CD vs. D	Rn Cytokines and Inflammatory Response Biocarta	17.4	92	6.497
	Rn IL-5 NetPath 17	7.6	98.5	4.28
	Rn Oxidative Stress	11.1	96.4	4.275
	Rn Fas Pathway and Stress Induction of HSP Regulation Biocarta	8.3	94.7	3.527
	Rn TGF beta Signalling Pathway	7	95.6	3.103
	Rn TGF beta Receptor NetPath 7	3.9	94.9	2.419
	Rn MAPK signalling pathway KEGG	3.8	95.6	2.399
CD vs. H	Rn Cytokines and Inflammatory Response Biocarta	30.4	92	3.373
	Rn Complement Activation Classical	35.7	100	3.296
	Rn Adipogenesis	18.2	91.7	3.231
	Rn IL-1 NetPath 13	22.2	97.3	2.555
	Rn Focal adhesion KEGG	14.3	87.5	2.032
	15 DAYS			
D vs. H	Rn Glycolysis and Gluconeogenesis	40.0	97.2	4.285
	Rn Electron Transport Chain	30.8	89.7	3.337
	Rn Androgen-Receptor NetPath 2	25.5	97	3.122
	Rn Proteasome Degradation	27.5	96.2	2.626
	Rn TNF-alpha NFkB NetPath 9	21.1	95.6	2.327
	Rn Complement Activation Classical	35.7	100	2.243
CD vs. D	Rn GPCRDB Other	7.7	62.9	2.74
	Rn T-Cell-Receptor NetPath 11	5.2	95.1	2.736
	Rn Wnt Signaling	7.3	93.2	2.63
	Rn IL-6 NetPath 18	5.3	97.9	2.532
CD vs. H	Rn Proteasome Degradation	31.4	96.2	4.51
	Rn Electron Transport Chain	28.8	89.7	3.977
	Rn Ribosomal Proteins	24.7	100	3.801
	Rn Glycolysis and Gluconeogenesis	31.4	97.2	3.734
	Rn Krebs-TCA Cycle	32	96.2	3.239
	Rn Wnt NetPath 8	22	92.9	3.209
	Rn Wnt Signaling	26.8	93.2	3.114
	Rn Nucleotide Metabolism	33.3	88.2	2.666
	Rn Androgen-Receptor NetPath 2	19.4	97	2.514
	Rn S1P Signaling	27.8	100	2.18
	Rn Complement Activation Classical	28.6	100	2.015

Table 5

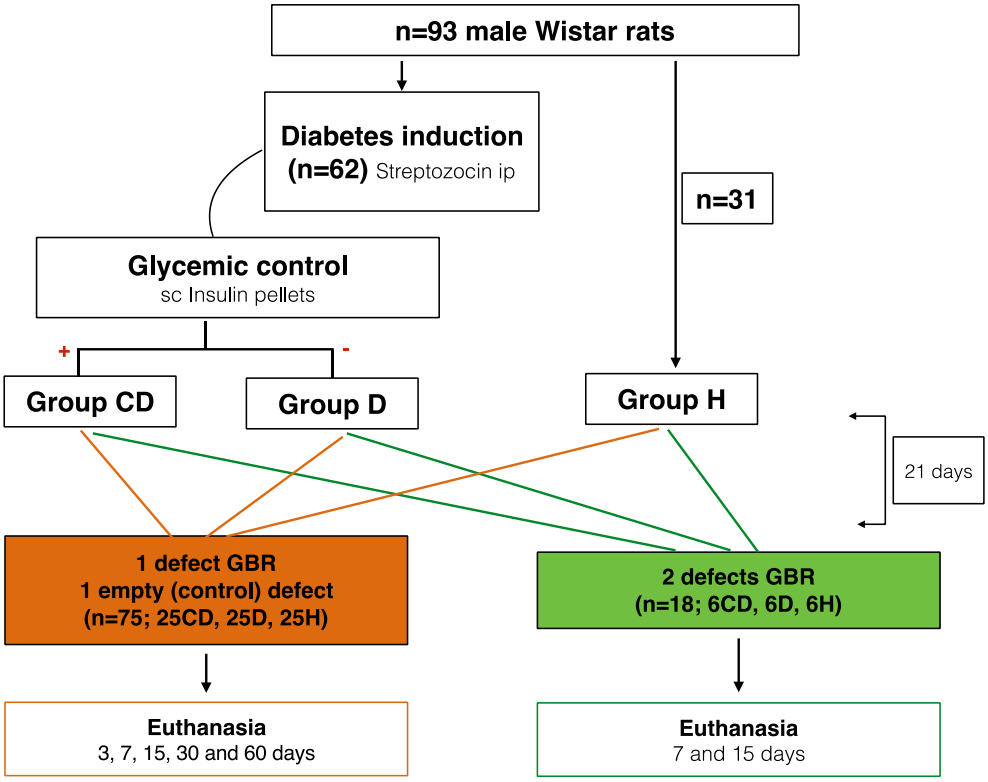
n=93 male Wistar rats
Diabetes induction
(n=62) Streptozocin ip
n=31
Glycemic control
sc Insulin pellets
+
-
Group CD
Group D
Group H
21 days
1 defect GBR
1 empty (control) defect
(n=75; 25CD, 25D, 25H)
2 defects GBR
(n=18; 6CD, 6D, 6H)
Euthanasia
3, 7, 15, 30 and 60 days
Euthanasia
7 and 15 days

Figure 1

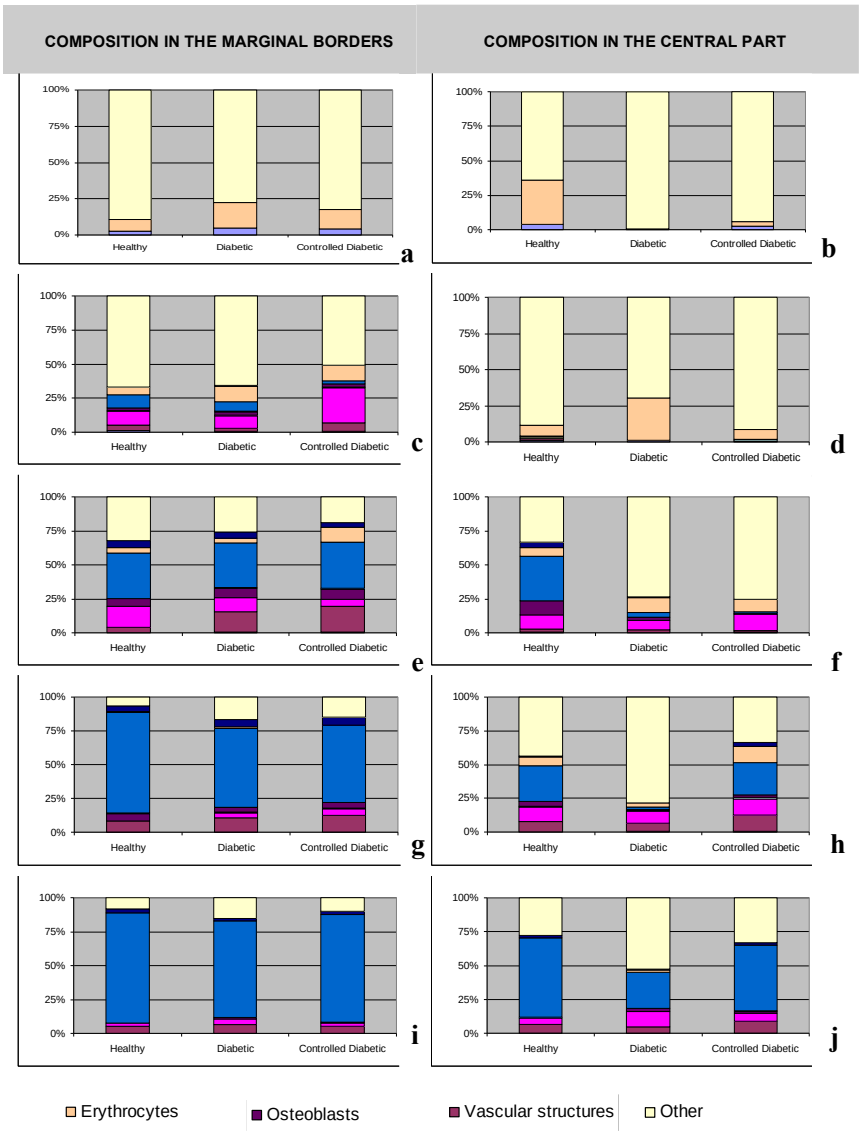

Figure 2

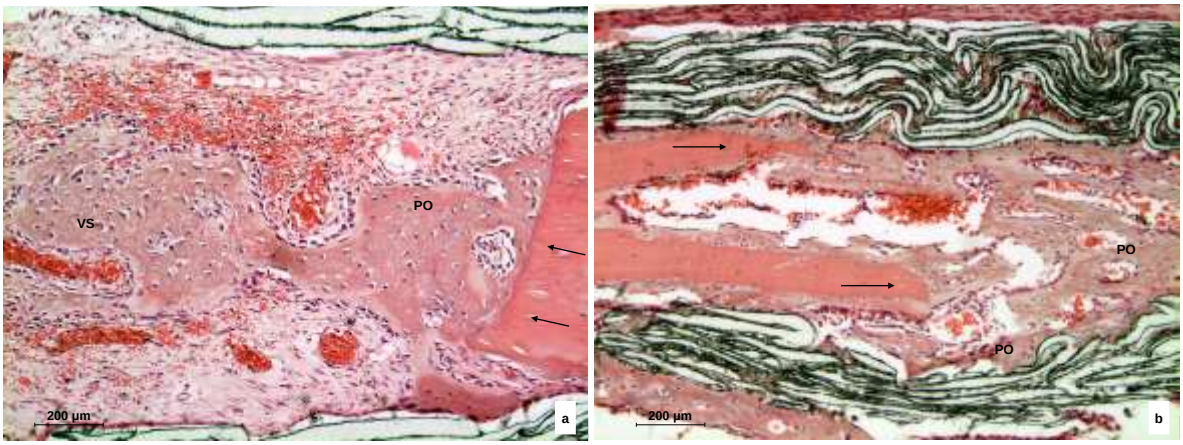

Figure 3

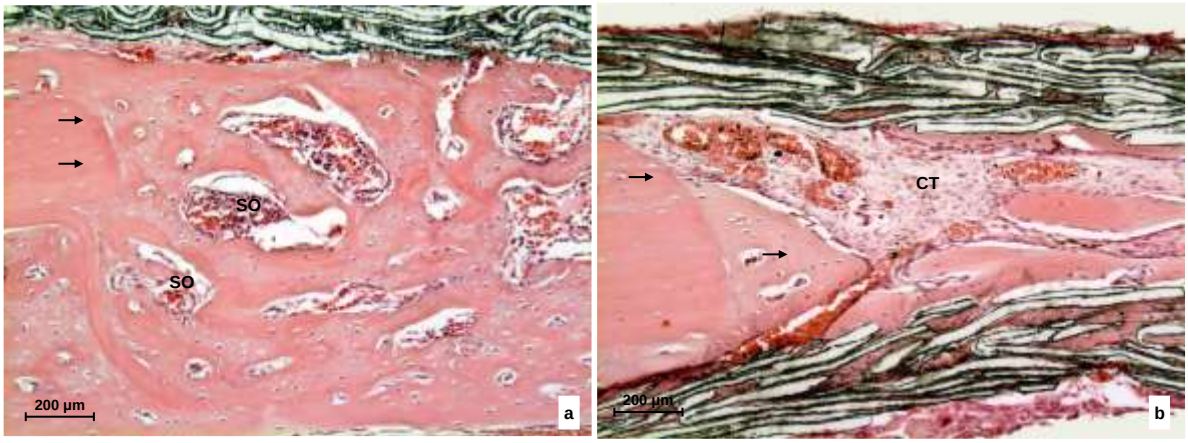

Figure 4

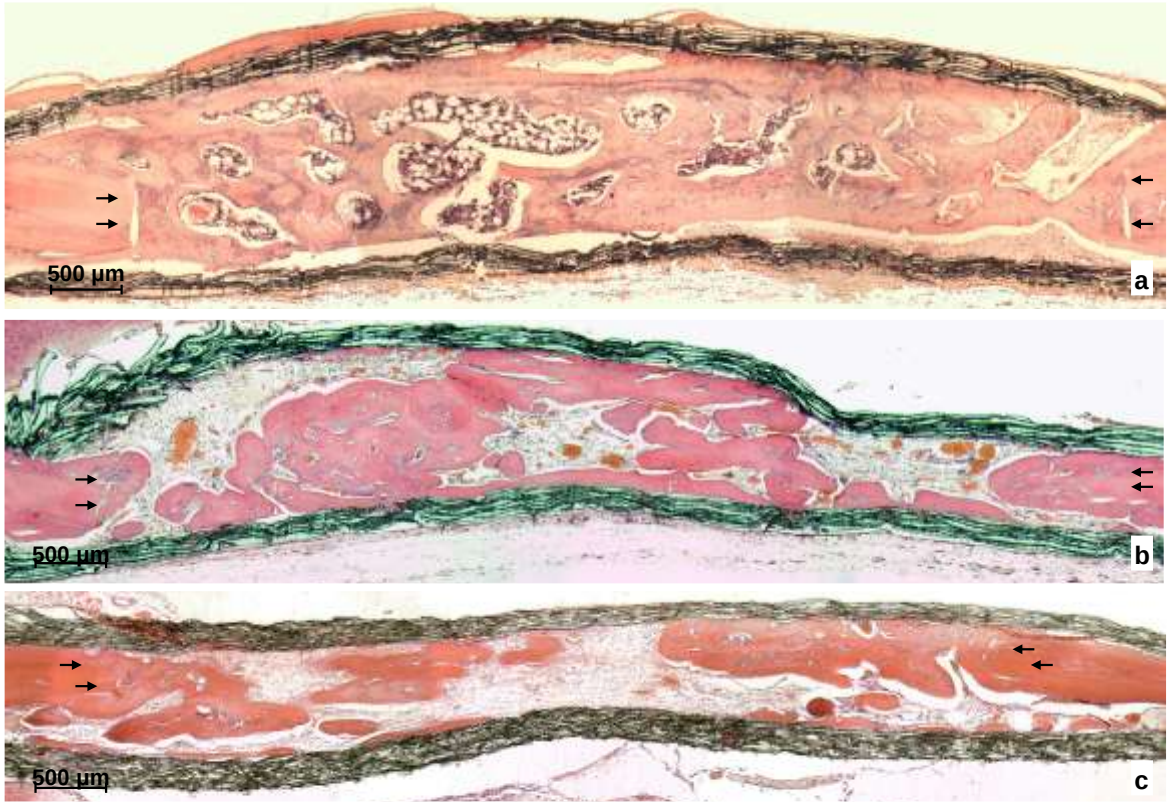

Figure 5